The Role of Convective Heating in Tropical Cyclone Eyewall Ring Evolution

CHUN-CHIEH WU, SHUN-NAN WU, AND HO-HSUAN WEI

Department of Atmospheric Sciences, National Taiwan University, Taipei, Taiwan

SERGIO F. ABARCA

Naval Postgraduate School, Monterey, California

(Manuscript received 15 March 2015, in final form 11 September 2015)

ABSTRACT

The purpose of this study is to analyze the role of diabatic heating in tropical cyclone ring structure evolution. A full-physics three-dimensional modeling framework is used to compare the results with two-dimensional modeling approaches and to point to limitations of the barotropic instability theory in predicting the storm vorticity structure configuration. A potential vorticity budget analysis reveals that diabatic heating is a leading-order term and that it is largely offset by potential vorticity advection. Sawyer–Eliassen integrations are used to diagnose the secondary circulation (and corresponding vorticity tendency) forced by prescribed heating. These integrations suggest that diabatic heating forces a secondary circulation (and associated vorticity tendency) that helps maintain the original ring structure in a feedback process. Sensitivity experiments of the Sawyer–Eliassen model reveal that the magnitude of the vorticity tendency is proportional to that of the prescribed heating, indicating that diabatic heating plays a critical role in adjusting and maintaining the eyewall ring.

1. Introduction

In contrast to the significant improvement in tropical cyclone (TC) track forecasts in the past few decades, the progress in TC intensity prediction has been limited (Wang and Wu 2004). Although advances have been made in our understanding of a variety of important topics regarding internal dynamics of TC intensity change, improvement in intensity prediction has been slow, in part because of limited understanding of the complicated dynamical processes involved. Examples of research topics on the dynamics of the storm's inner core are vortex Rossby waves (Guinn and Schubert 1993; Montgomery and Kallenbach 1997; Möller and Montgomery 1999), spiral rainbands, mesoscale vortices (Hendricks et al. 2004; Montgomery et al. 2006; Van Sang et al. 2008), and eyewall processes (Willoughby et al. 1982; Huang et al. 2012). Changes in storm intensity are usually accompanied by changes in the eyewall structure. Kossin and Eastin (2001) analyzed the transformations of eyewall structure, as captured by aircraft observations of Hurricanes Oliva (1994) and Diana (1984). The authors showed that during the storm's weakening after reaching its peak intensity, the pattern of angular momentum and potential temperature tends to shift from a ring shape to a monopole.

The evolution of TC structure is affected by several factors, such as convective heating or wave dynamics. A series of studies (Schubert et al. 1999; Kossin and Schubert 2001; Hendricks et al. 2009; Hendricks and Schubert 2010) have discussed the impact of barotropic instability on the TC-like vorticity ring evolution based on the linear stability theory in an unforced-barotropic model. It has been shown (Schubert et al. 1999) that when the distribution of vorticity satisfies the Charney–Stern condition, barotropic instability occurs. Both the thickness (the width of the ring) and the hollowness (the difference in vorticity between the eye and eyewall) of a vorticity ring structure have been identified as determining the development of the unstable mode. The results suggested that the TC-like vorticity ring structure would experience barotropic instability and collapse into mesovortices (with several separated coherent

Corresponding author address: Chun-Chieh Wu, Department of Atmospheric Sciences, National Taiwan University, No. 1, Sec. 4, Roosevelt Rd., Taipei 10617, Taiwan.
E-mail: cwu@typhoon.as.ntu.edu.tw

DOI: 10.1175/JAS-D-15-0085.1

vorticity patches that continued to circulate cyclonically around an annulus center) or into a monopole (with the vorticity maximum at the circulation center and decreasing values with radius).

In addition to the dynamical processes, storm thermodynamics also plays an important role in the TC structure evolution. Studies based on highly idealized integrations point to the importance of diabatic heating in maintaining a ringlike structure in the TC. Rozoff et al. (2009) used a prescribed annular vorticity source (aimed to mimic the azimuthal-mean component of asymmetric convection in a real TC) in a forced-barotropic nondivergent model to assess the influence of the heating source on the ring structure evolution. The results showed that the presence of a heating source can maintain the ring structure under the barotropically unstable condition. Hendricks et al. (2014) used a shallow-water model to evaluate the impact of the convergence due to diabatic heating as the vorticity source. Their results are, in part, consistent with the finding of Wu et al. (2009), as they found that, with relatively large diabatic heating, the ring can persist and that, without enough forcing, the thin ring structure would break down into mesovortices. Both Rozoff et al. (2009) and Hendricks et al. (2014) indicated that the influence of diabatic heating is significant and nonnegligible. While the Hendricks et al. (2014) modeling strategy represents a bridge between two-dimensional (2D) forced-barotropic frameworks and three-dimensional (3D) full-physics models, the issue has not been addressed from the full three-dimensional perspective.

Three-dimensional full-physics modeling studies have been conducted to examine the evolution of TC structures (e.g., Yau et al. 2004; Wang 2009; Wu et al. 2009; Nguyen et al. 2011; Naylor and Schecter 2014). In the simulation of Typhoon Zeb (1998), the sustained ring structure can be simulated in the full-physics model. Wu et al. (2009) further elucidated the roles of both condensation heating and friction in maintaining the potential vorticity (PV) ring. They showed that the diabatic heating is important in sustaining the PV ring, yet the surface friction plays a dual role in affecting the annular PV structure evolution. On one hand, the friction dissipates PV in the eyewall; on the other hand, it helps keep the narrow PV ring by increasing the stretching deformation in the boundary layer. Naylor and Schecter (2014) conducted simulations with a cloud-resolving model (with 250-m horizontal grid spacing) and evaluated the influence of the moist convection on TCs by adjusting the ratio of the exchange coefficients of enthalpy and momentum. They showed that, even though the convective heating exists, the initial ring vortex would break down as a result of barotropic instability during the intensification stage of the TC.

In short, many studies have investigated the eyewall ring evolution in 2D dry models. However, these highly idealized models have their limitations in investigating eyewall dynamics, in which moist convective processes may be very important. Although a simulation based on barotropic models with a prescribed heating can suggest the importance of the diabatic heating, its prescribed heating in a 2D model is simplistic. Diabatic heating in nature, resulting from multiscale three-dimensional processes, often exhibits a distinct vertical profile in convective regions that will impact the three-dimensional structure of vorticity generation. To address the above issues, a full-physics numerical model is used in this study to investigate the role of the diabatic heating in maintaining the eyewall ring structure as the TC reaches the mature stage. This study examines the role of the convective heating, including the feedback with the eyewall convective structure, which has not been considered in previous published studies. Several sensitivity simulations are conducted to explore the effect of convective heating on the maintenance of the annular PV structure. The model settings and experimental design are addressed in section 2. Sections 3 and 4 illustrate the results from the full-physics model as well as from a balanced model and further analyze the role of convective heating in affecting the TC structure evolution. The major findings and a summary of this study are presented in section 5.

2. Model and experiment design

The two models used in this study are a three-dimensional full-physics model and a highly idealized two-dimensional diagnostic model.

a. 3D full-physics model

The Advanced Research Weather Research and Forecasting (WRF) Model (ARW; version 3.3.1) is adopted to simulate the TC-like vortex evolution in a quiescent environment (Skamarock et al. 2008). The horizontal grid resolution is 3 km with 401 $\times$ 401 grid points, and the grid meshes include 34 eta levels. Unlike in the WRF real case simulation, the idealized setting adopts periodic boundary conditions, and the initial vortex structure is based on Rotunno and Emanuel (1987). During the entire integration time, the sea surface temperature is fixed at 29°C, and the simulation is on an f plane at 15°N without terrain. The Mellor–Yamada–Janjić (MYJ) TKE PBL scheme (Janjić 2001) is used for boundary layer parameterization, and the WRF single-moment 3-class (WSM3) simple ice scheme

(Hong et al. 2004) is used for microphysics parameterization. With the setup of high horizontal resolution, the cumulus parameterization is not employed. The Jordan sounding (Jordan 1958) is used as the initial atmospheric temperature and humidity conditions.

This study focuses on the TC structure evolution after its intensity reaches a quasi-steady (mature) state. To obtain the steady-state ring structure within the unstable flow regime, the TC-like vortex ring after a 180-h prerun is used as an initial vortex for the 100-h control simulation (CTL). Sensitivity experiments are carried out to assess the impact of convective heating on the PV structure. In these sensitivity experiments, convective heating (in the microphysics scheme) is adjusted by a constant factor at each grid point in the domain throughout the integration. Those experiments integrated with diabatic heating multiplied by a factor of 1.2, 0.8, and 0.5 are denoted as LH12, LH08, and LH05, respectively.

b. Balanced model

Another model used in this study is a thermal wind balanced model based on the Sawyer–Eliassen (SE) equation (Eliassen 1951; Shapiro and Willoughby 1982; Schubert and Hack; 1983; Hack and Schubert 1986). Essentially, the SE equation solves for the secondary circulation that a balanced vortex would develop when forced by diabatic heating or friction in order to remain in balance. Numerous studies have used the SE model to diagnose the effects of external forcing on TC evolution and secondary eyewall (e.g., Bui et al. 2009; Rozoff et al. 2012; Abarca and Montgomery 2014, 2015).

In this study, the quantities used to define the vortex and its forcing in the SE model are derived from WRF output, as described in section 4 below. We use the SE model to diagnose the axisymmetric secondary circulation with which the balanced vortex responds to the given annular heat source. We note that the SE boundary conditions are characterized by streamfunction values equal to zero. The equation is solved by numerical inversion, using the successive over relaxation scheme.

3. 3D full-physics model analyses

A mature vortex is provided for the control and sensitivity simulations in this study. The mature vortex is extracted from the result of a prerun integration, as described in section 2a. During the next 100 h of integration time, the maximum azimuthal-mean tangential velocity remains steady near $70\,\mathrm{m\,s^{-1}}$, with the maximum vorticity around $6 \times 10^{-3}\,\mathrm{s^{-1}}$. The following analysis focuses on the evolution of the storm's ring structure after the TC vortex reaches the mature stage.

a. Linear stability analysis and its limitations

First, we examine the presented simulation under the light of the barotropic instability theory of Schubert et al. (1999). The parameters of this theory, the thickness and hollowness (δ and γ, which are defined as the width of the ring and the difference in vorticity between the eye and eyewall, respectively) of the initial ring are obtained. These quantities are computed from the azimuthal-mean vorticity at three vertical levels. The three levels chosen are 0.6-km height (representing the boundary layer of the storm), 3-km height (the region between boundary layer and largest diabatic heating), and 6-km height (which corresponds to the level of largest diabatic heating).

Figure 1 shows that the parameters corresponding to the vortex structure at 0.6 km are $\gamma = 0.53$ and $\delta = 0.61$, indicating that the highest growth rate is located in the area of wavenumber 4 with an *e*-folding time around 43.7 min [calculated from Eq. 2.11 in Schubert et al. (1999)]. The figure also shows that, at the height of 3 km, the parameters are $\gamma = 0.68$ and $\delta = 0.74$, with the fast-growing mode in wavenumber 6, with an *e*-folding time around 167 min; at 6-km height, the vortex structure prescribed as $\gamma = 0.67$ and $\delta = 0.66$ suggests that the *e*-folding time under the fast-growing mode and in the area of wavenumber 5 is 104 min. These results indicate that the initial profile in our simulation is well within the barotropically unstable profile.

According to linear stability theory, given that our profiles are in an unstable regime, the vorticity structure distributions at 0.6, 3, and 6 km should all be in the form of small scattered patches instead of the PV field exhibiting a ring structure. However, such scattered patch structure is not present in the 3D full-physics model integration. Our comparisons, along with previous research based on forced-barotropic models (Rozoff et al. 2009; Hendricks et al. 2014) and 3D full-physics models (Wu et al. 2009), suggest that the strikingly different evolution observed between the unforced-barotropic framework and the 3D integrations is not only because of the geometrical (2D vs 3D) configuration but is also related to the effects of diabatic heating, absent in the unforced-barotropic model.

b. Ring structure evolution

In this section, PV distribution is examined to show the evolution of the eyewall ring. Section 3a showed that, although the initial ring structure is located in a barotropically unstable flow regime, the eyewall ring in CTL is maintained through the integration. While

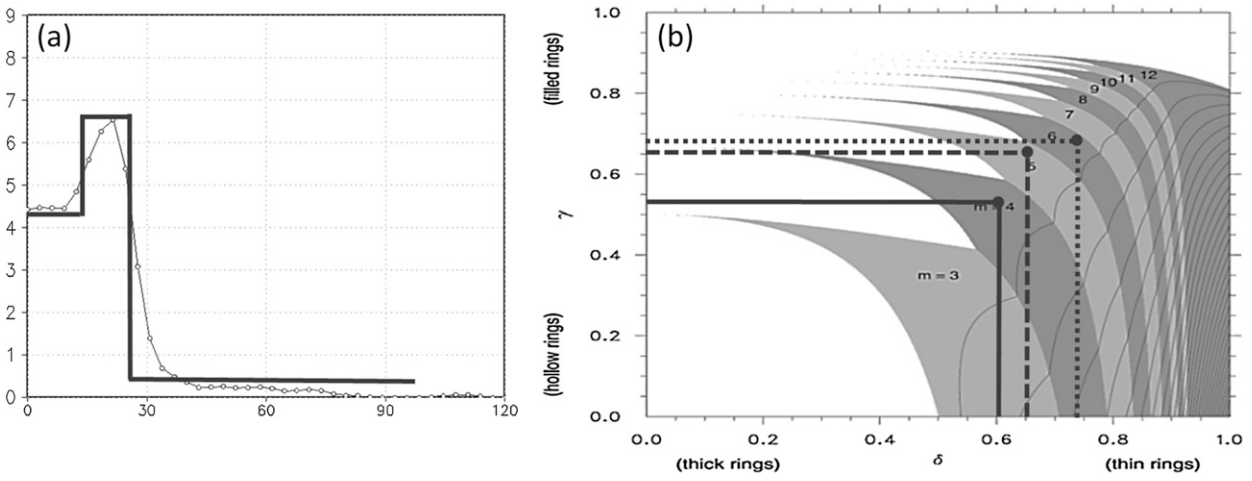

FIG. 1. (a) The azimuthal mean of relative vorticity (10^{-3} s^{-1}) in the initial vortex at $z = 3$ km (thin line) and the corresponding vorticity profile (thick line), as discussed in Schubert et al. (1999). (b) Taken from Fig. 2 in Hendricks et al. (2009). The wavenumber with the greatest dimensionless growth rate at 3 km (short-dashed line), which is determined by the nondimensional parameters γ (width of the ring) and δ (difference in vorticity between eye and eyewall), corresponding to the vortex structure shown in (a); the wavenumber with the greatest dimensionless growth rate at 0.6 (solid line) and 6 km (short-dashed line).

asymmetric disturbances do occur in some time periods during the model integration, there is no evidence of significant growth in asymmetry due to barotropic instability in the simulation. We suggest that the presence of diabatic heating may have contributed to the maintenance of the PV ring and that, to assess the impact of convective heating on the PV ring, further sensitivity experiments on convective heating should be carried out following the design in section 2a.

The evolution of the PV ring (at $z = 3$ km) in the sensitivity experiments is shown in Figs. 2 and 3. The PV ring with the largest diabatic heating (LH12) persists throughout the integration, with larger maximum values of potential vorticity than CTL (Figs. 2d–f, 3b). The PV ring with the least diabatic heating (LH05) considered becomes a monopole and dissipates within 1 day of integration (Figs. 2j–l, 3d). The PV ring in LH08, with slightly reduced convective heating (with respect to CTL) also sustains its PV initial configuration, while the intensity on the ring becomes weaker than CTL (Figs. 2g–i, 3c). At 6-km height (not shown), LH08 shows an evolution different from those at 3 km. The PV ring of LH08 initially transforms to a monopole, but, different from LH05, the ring structure recovers afterward and remains as such until the end of the integration. At the height of 0.6 km (not shown), though this layer is largely influenced by the frictional effect, the evolution of the different PV rings analyzed is like those at 3 km.

To narrow down the critical value (fraction of convective heating) that determines whether or not there is a transition to a monopole, we have conducted simulations by multiplying the diabatic heating by a factor of 75%, 70%, 65%, and 60%, respectively. The results in the sensitivity simulations with diabatic heating multiplied by 75% and 70% are similar to those in LH08 (with the PV on the ring being only slightly weaker than LH08). In contrast, when the fraction of convective heating is below 65%, the vortex ring transforms into a monopole structure, which is the same as the result in LH05.

As we examine the horizontal plot of diabatic heating in CTL and LH08 at the beginning of the simulations (not shown), vorticity generation in CTL usually shows an annular distribution. On the other hand, the pattern of diabatic heating in LH08 demonstrates a crescent shape without an organized ring structure most of the integration time, and the asymmetric heating source would lead to the growth of asymmetries.

The simulations described in this section indicate the importance of 3D convective heating processes in the evolution of realistic TC eyewall rings and highlight the differences between results obtained from the 3D processes and the 2D unforced-barotropic models. The sensitivity experiments discussed above confirm that diabatic heating is important to the maintenance of the ring structure. Note that simulations without enough diabatic heating, such as LH05 and those integrated with the heating multiplied by 0.65 and 0.60, cannot sustain the ring heating structure. This result is different to that in Naylor and Schecter (2014), which indicated that a ringlike vortex cannot sustain itself in the presence of diabatic heating (although we note that their study focused on the intensification period, which

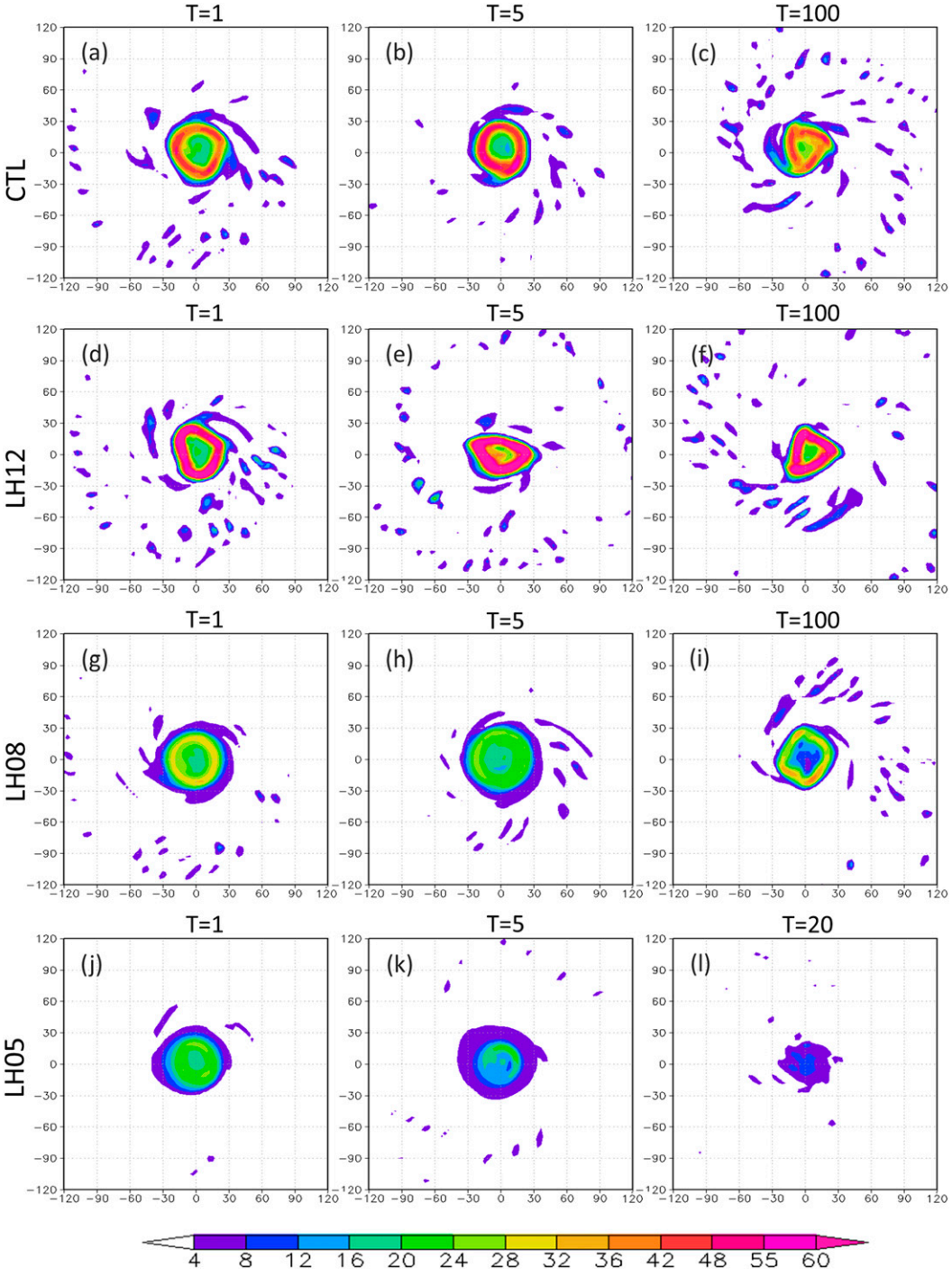

FIG. 2. The evolution of the potential vorticity ring (PVU; 1 PVU = 10^{-6} K kg^{-1} m^2 s^{-1}) at z = 3 km at (left) 1, (center) 5, and (right) 100 h for (a)–(c) CTL; (d)–(f) LH12; (g)–(i) LH08; (j),(k) LH05; and (l) at 20 h for LH05, as the vortex has already dissipated at 100 h.

is different from our analyses of the TC vortex at the mature stage with steady vortex intensity and structure). One of the possible reasons for different evolutions between this work and that of Naylor and Schecter (2014) is the asymmetric or disorganized distribution of diabatic heating, which would generate uneven vorticity patches that contributes to the breakdown of the ring structure.

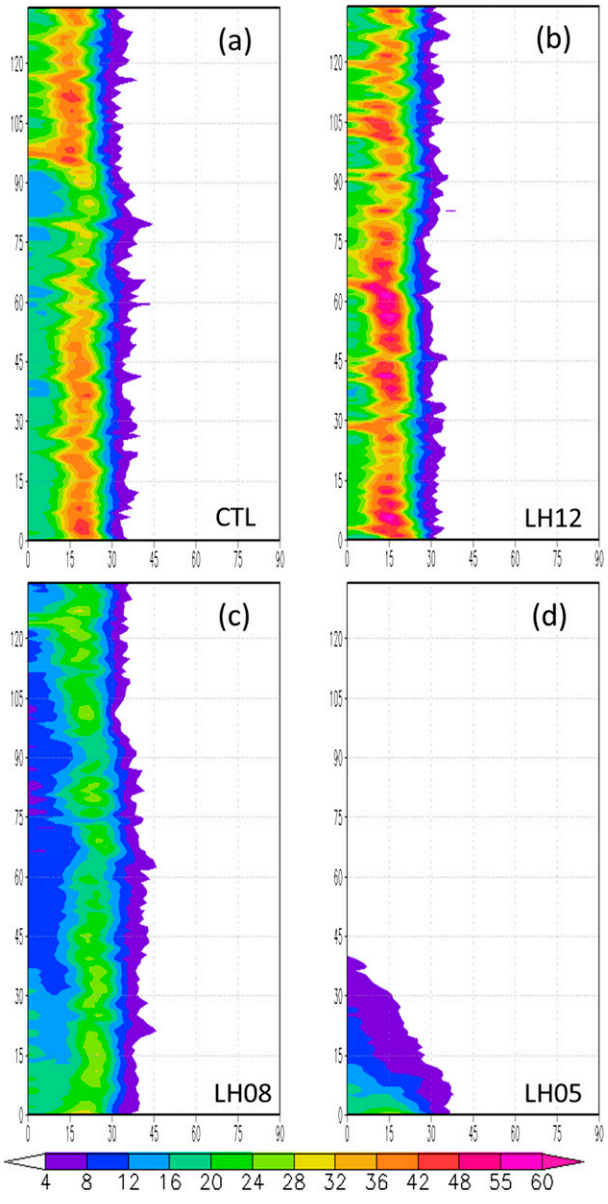

FIG. 3. The time evolution (h) of the azimuthal mean of potential vorticity (PVU) at each radius in (a) CTL, (b) LH12, (c) LH08, and (d) LH05 at $z = 3$ km.

c. PV budget analysis

We now focus on the role of diabatic heating in maintaining the PV ring during the vortex's mature stage. PV budget analyses are conducted to investigate the mechanism that helps maintain the eyewall PV ring. The azimuthal mean of the PV equation is

$$\frac{\partial \overline{P}}{\partial t} = -\overline{V \cdot \nabla P} + \overline{\frac{1}{\rho}\boldsymbol{\eta} \cdot \nabla \dot{\theta}} + \overline{\frac{1}{\rho}(\nabla \times F) \cdot \nabla \theta}, \qquad (1)$$

where P stands for potential vorticity; θ and $\dot{\theta}$ are potential temperature and diabatic heating, respectively; $\boldsymbol{\eta}$ is the absolute vorticity vector; F is frictional force; and the bar refers to the azimuthal mean. On the right-hand side of the equation, the three terms indicate contributions from advection, diabatic heating, and friction, respectively. On the left-hand side is the simulated PV tendency. Here, we focus on evaluating the effect of convective heating and therefore neglect the influence of friction, which can substantially affect the budget in the boundary layer.

Figure 4 shows the azimuthal-mean PV budget terms at 8 h in LH05 (Figs. 4a–c), LH08 (Figs. 4d–f), CTL (Figs. 4g–i), and LH12 (Figs. 4j–l). The figure shows large variability among the simulations at the time shown. However, in all experiments, the diabatic heating and advection terms are one order larger than the corresponding tendency term. In each case the PV generation associated with diabatic heating is substantially large and largely offset by the advection, leading to a relatively small PV tendency. The simulated PV tendency in LH12 is larger than that in CTL, particularly the positive tendency near the ring (the ring region is about 8–24-km radius for LH12), while LH08 shows a small negative tendency near the ring area (the ring area is about 15–30-km radius in LH08), indicating slight weakening of the ring intensity. In LH05, the ring structure cannot be maintained in the simulation, and a negative tendency is found in the simulated PV in most areas. These results suggest that contributions from both diabatic heating and advection become more significant as latent heat release increases.

The above results suggest that larger diabatic heating can better maintain the ring structure, even though the increased contribution from diabatic heating to the PV generation is largely offset by the stronger advection corresponding to the enhanced diabatic heating.

d. Impact time scale of diabatic heating and advection of PV

In section 3a, we found that the ring structure evolution of the WRF Model is substantially different from those based on an unforced-barotropic framework. Here, in addition to the PV budget analysis, we calculate the *e*-folding time of the terms in the PV equation based on results from CTL. Also, the *e*-folding time under the fastest-growing mode of barotropic instability is calculated based on Schubert et al. 1999. While the *e*-folding time associated with barotropic instability is approximately 167 min for the rings at 3 km, the *e*-folding time associated with the advection and diabatic heating terms around the eyewall region can be less than 10 min in our

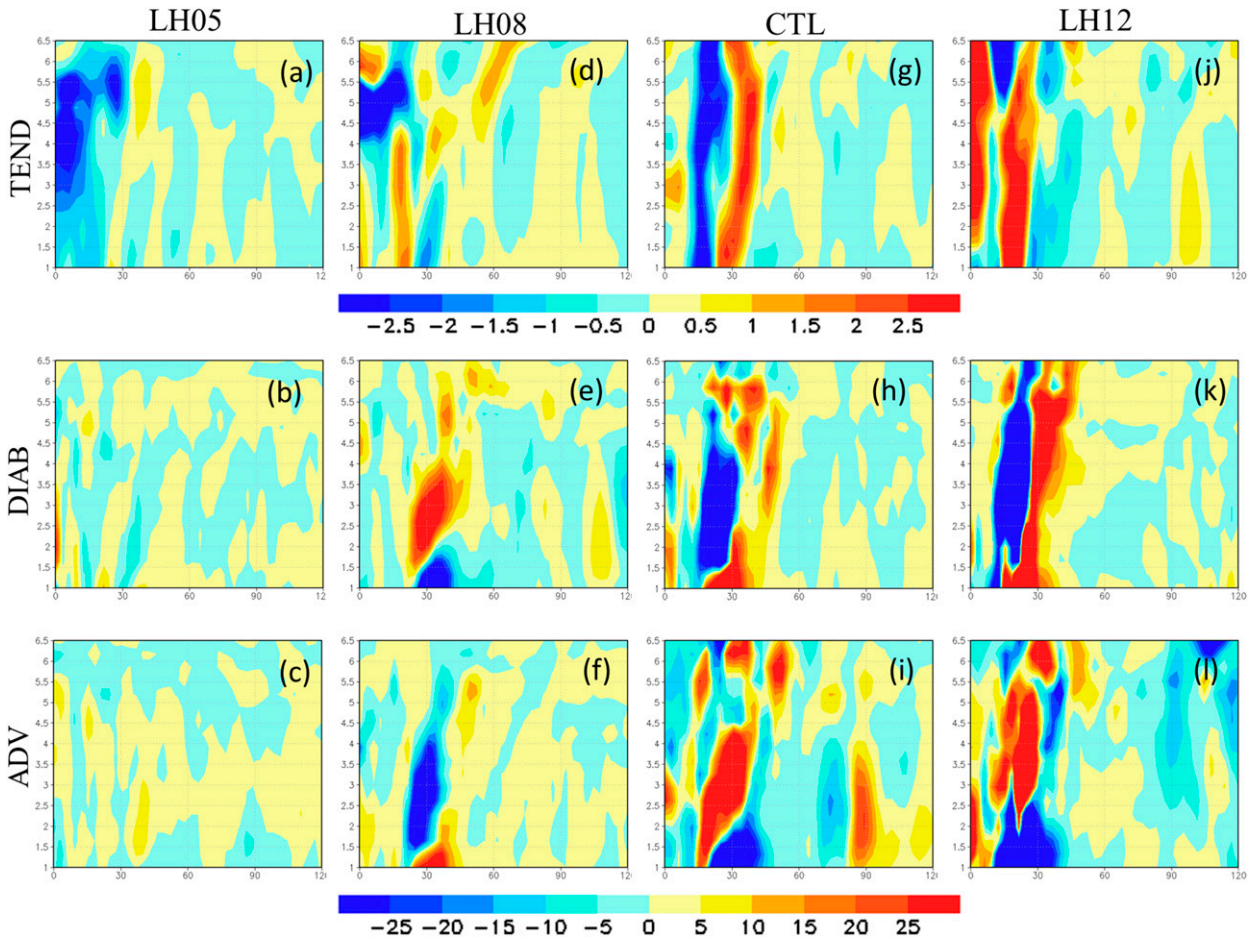

FIG. 4. The radius–height (km) cross section of the azimuthally averaged potential vorticity budget analysis (PVU h^{-1}) at 8 h: (top) simulated tendency term, (middle) diabatic heating term, and (bottom) advection term for (a)–(c) LH05; (d)–(f) LH08; (g)–(i) CTL; and (j)–(l) LH12.

CTL simulation, as shown in Fig. 5. The results show that strengthening of the PV ring through the integral effect of both advection and heating is more effective than its weakening through barotropic instability. The disturbance from barotropic instability does not intensify over time and is always accompanied by fast adjustments of advection and diabatic heating.

While the contribution from diabatic heating in maintaining the ring structure is largely offset by advection, it still plays an important role in sustaining the ring structure. To understand this role, we use the SE model to diagnose the secondary circulation and then investigate the effect of an induced secondary circulation on the structure evolution in the mature TC.

4. Sawyer–Eliassen model diagnoses

To further understand the impact of diabatic heating on the evolution of eyewall ring structure, the SE equation (Eliassen 1951; Shapiro and Willoughby 1982; Hack and Schubert 1986) is used. In our case, the equation is used to diagnose the secondary circulation in response to the diabatic heating in isolation from boundary layer processes. We do not include frictional forcing either on the SE equation integration or in the postprocessing of the secondary circulation generated by the model. Ignoring the boundary layer processes allows us to focus on the effects of diabatic heating without adding complications that could potentially obscure the results.

a. WRF output diagnoses

To solve the SE equation, we use a balanced vortex characterized by the azimuthal-mean pressure and density fields from the CTL simulation along with the corresponding gradient wind field. We find that the gradient wind is very close to the mean tangential wind, with most differences being less than 10%, except in the boundary

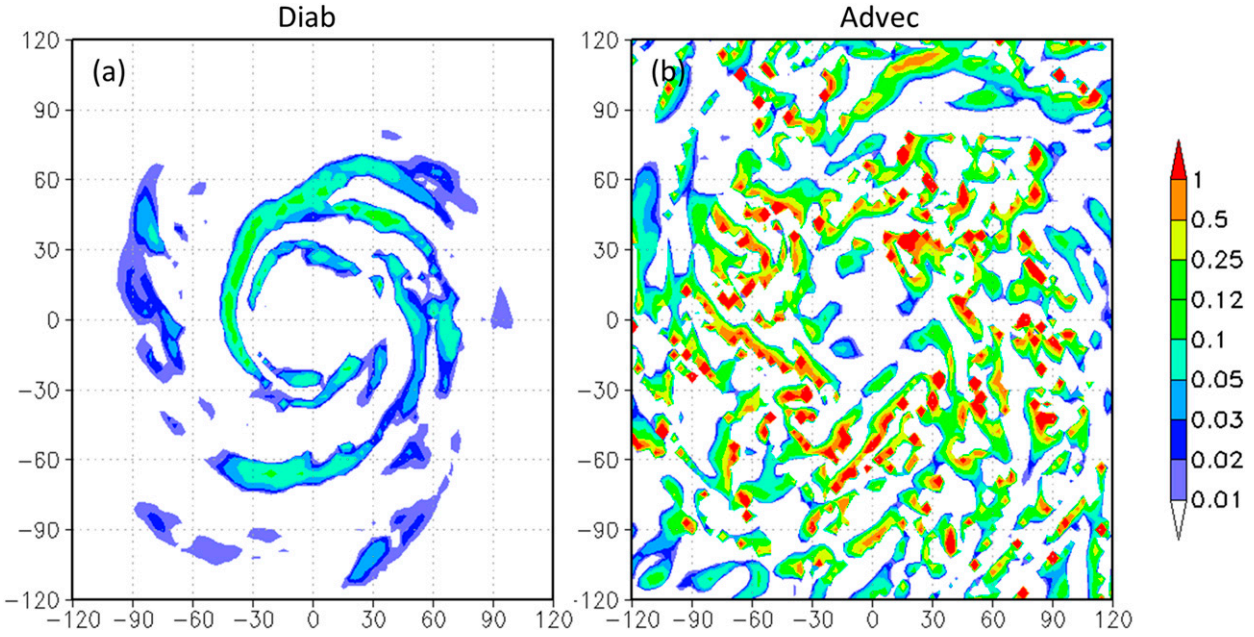

FIG. 5. The *e*-folding time (min) of the (a) diabatic heating term and (b) advection term at $z = 3$ km in CTL.

layer, where departures from gradient wind balance can be large and potentially relevant in storm dynamics (Bui et al. 2009; Abarca and Montgomery 2014, 2015). Similarly, the diabatic heating profile used in the SE model is acquired from WRF Model simulations.

Figure 6 shows that the inflow diagnosed with the SE equation is weaker than that of WRF in the boundary layer. Above the boundary layer, the inflow diagnosed with the SE equation alternates between being somewhat larger and somewhat smaller compared with that of the WRF Model. Around the eyewall region, compared with the WRF Model flow, the upward vertical velocity diagnosed with the SE equation is weaker in magnitude but broader in radial extent.

We compute the relative vorticity tendency from the secondary circulation diagnosed by the SE equation. For this computation, we first obtain the tangential wind tendency associated with the radial and vertical advection of tangential momentum (ignoring friction) and calculate relative vorticity as

$$\frac{\partial}{\partial t}(\zeta) = \frac{(\partial v/\partial t)}{r} + \frac{\partial(\partial v/\partial t)}{\partial r}, \tag{2}$$

where ζ and v stand for relative vorticity and tangential velocity, respectively, and the rest of the symbols are conventional.

At the altitudes of 0.6, 3, and 6 km, the diagnosed vorticity tendency shows a ringlike pattern, and the largest positive vorticity tendency is located in the area of the vorticity ring. This analysis suggests that the vorticity tendency induced by the secondary circulation would help maintain the original ring structure.

Furthermore, we adopt the SE model to conduct a series of sensitivity tests to identify the impacts of different strengths of diabatic heating on ring structure evolutions (Fig. 7). Comparing the results associated with full (CTL) and half (LH05) WRF output heating profiles, we note that the difference in diagnosed vorticity tendency between different magnitudes of the heating source exhibits a ringlike shape. This ringlike difference implies that the eyewall has stronger positive vorticity tendency on (and slightly outside) the ring when provided with more diabatic heating, thus helping maintain and enhance its annular vorticity.

Consequently, different magnitudes of diabatic heating induce corresponding vorticity tendencies, and a stronger strength of diabatic heating provides more favorable conditions for the maintenance of the ring structure. Although the SE model is a diagnostic model and does not contain the physical process for simulating barotropic instability, this finding associated with the SE model is consistent with the results in section 3 and contributes to explaining why experiments with larger diabatic heating, such as CTL, have greater potential in maintaining the ring structure, whereas experiments with smaller diabatic heating,

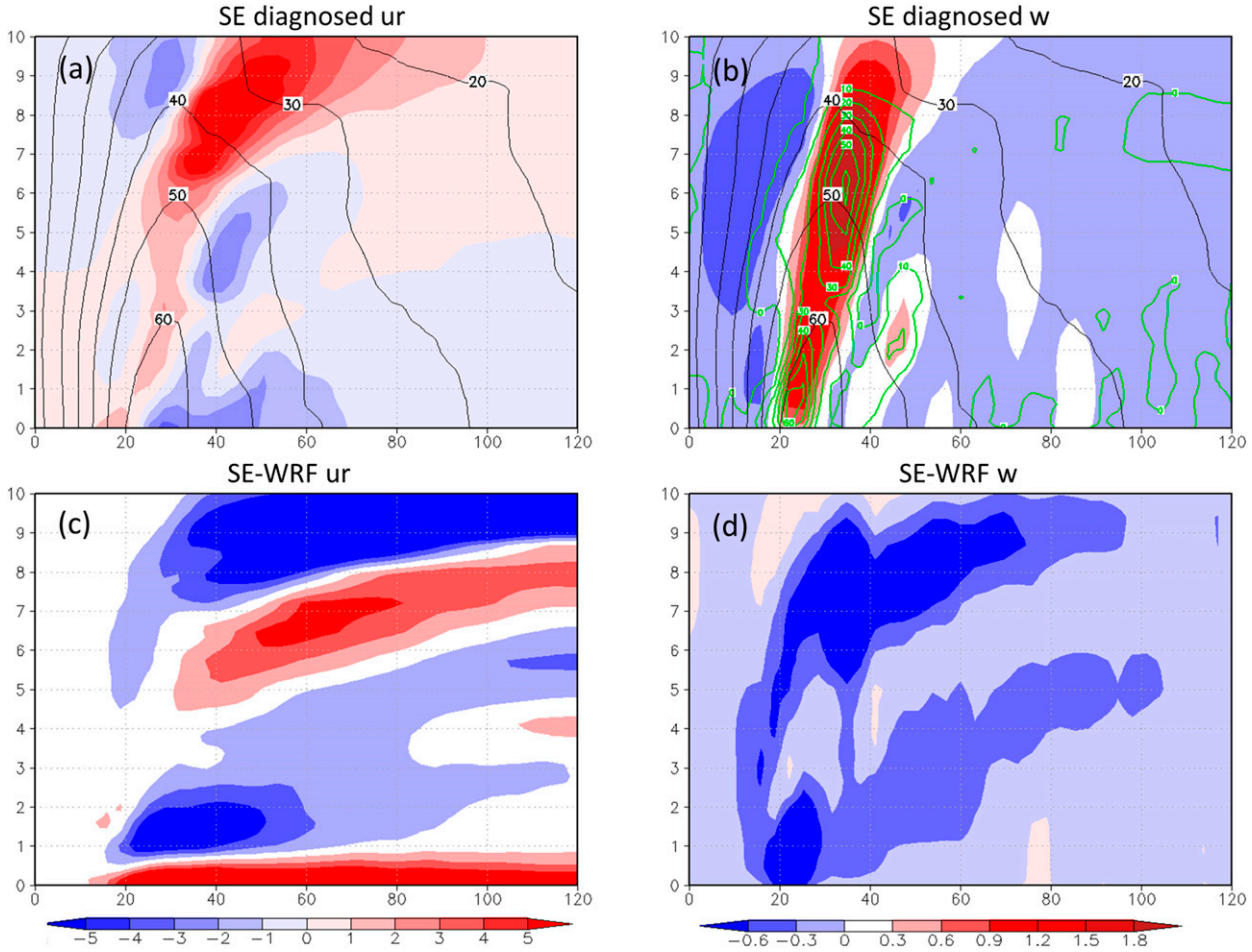

FIG. 6. The radius–height (km) plots of the SE model with diagnosed (a) radial velocity ($m\,s^{-1}$) and (b) vertical velocity ($m\,s^{-1}$), tangential velocity ($m\,s^{-1}$; black lines), and diabatic heating ($K\,h^{-1}$; green lines) that is larger than $0\,K\,h^{-1}$. The difference in (c) radial velocity ($m\,s^{-1}$) and (d) vertical velocity ($m\,s^{-1}$) between the SE-diagnosed and WRF output (SE minus WRF).

such as LH05, tend to exhibit an annular structure that evolves to a monopole.

b. Sensitivity to the initial ring structure

While the significant difference between diagnosed relative vorticity tendencies related to different diabatic heating is found, it is of interest to investigate the influence of the initial TC structure on the vorticity ring evolution with the presence of diabatic heating.

Following the framework (Schubert et al. 1999) on barotropic instability of the TC vortex, we build up a radial vorticity profile within the regime of the unstable ring structure at the altitude of 3 km (iCTL). The structure of initial vorticity and the maximum value of diabatic heating are specified to be similar to those in WRF output. The maximum vorticity of about $6.5 \times 10^{-3}\,s^{-1}$ is located at 15 km in radius with a ring width of about 12 km, and the vorticity difference between the ring and the inner core is $3.5 \times 10^{-3}\,s^{-1}$ (Fig. 8a). Also, the diabatic heating profile is derived from the 3-h time- and azimuthal-mean WRF output. The results from the SE diagnostics show that the maximum positive vorticity tendency in iCTL is just slightly weaker than those in response to WRF output with full diabatic heating, and the pattern of vorticity tendency also shows a ringlike distribution with its positive vorticity tendency collocated with (and slightly outside) the vorticity ring.

Furthermore, we modify the size or shape of the ring to specify three other vortex structures with a narrower ring (NR; with width around 9 km), a wider ring (WD; with width around 18 km), and less vorticity difference between the center and the ring (LD; with difference of about $1.5 \times 10^{-3}\,s^{-1}$), as shown in Fig. 9. Following the linear stability theory, the NR ring structure is located in the unstable regime, while both WD and LD are in the

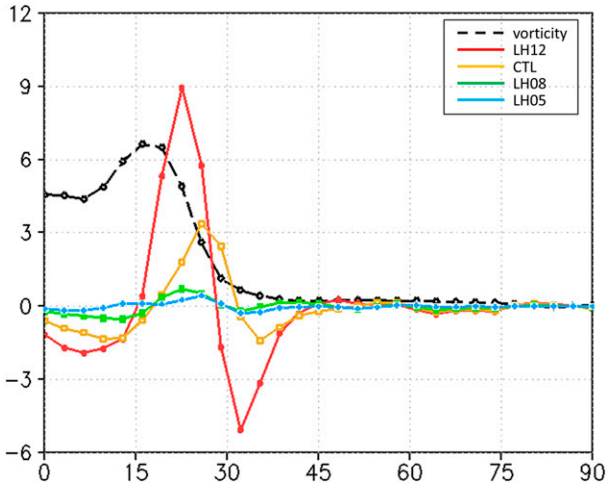

FIG. 7. The radial profile of relative vorticity ($s^{-1} \times 10^{-3}$; black dashed line) from WRF output at $z = 3$ km. The four colored solid lines represent the SE model with diagnosed relative vorticity tendency ($s^{-1}\,h^{-1} \times 10^{-3}$) associated with 3-h time- and azimuthal-mean heating forcing of LH12 (red), CTL (yellow), LH08 (green), and LH05 (blue).

stable regime. Because WD and LD ring structures are within the stable regime, not surprisingly, the diagnosed vorticity tendencies demonstrate a ringlike structure. On the other hand, although the vortex structure in NR is located in the unstable flow regime, the diagnosed vorticity tendency still shows an annular distribution that can help maintain the ring structure. These sensitivity experiments indicate that, with the aid of diabatic heating, the annular vorticity can be maintained even in experiments with the initial vorticity structure in an unstable flow regime.

With different initial vortex structures, previous researchers demonstrated that most evolutions of ring structures ended in monopole or with several vortices under adiabatic conditions (Schubert et al. 1999; Kossin and Schubert 2001; Hendricks et al. 2009; Hendricks and Schubert 2010). However, the convective heating is an important energy source to the real TC, and the SE model distinctly shows that most ring structures can be sustained with sufficient diabatic heating. Therefore, we suggest that diabatic heating is capable of adjusting the ring structure, showing its important role in maintaining the ring structure.

5. Summary

In this study, idealized simulations based on the WRF Model are carried out to investigate the mechanisms behind the evolution and maintenance of the tropical cyclone eyewall ring configuration. It is shown that the presence of convective heating in the eyewall plays an important role in maintaining the ring structure when the tropical cyclone intensity is at a mature stage. This result is consistent with previous research based on forced-barotropic and shallow-water models. We show also that the convective heating generates positive potential vorticity in and slightly outside the ring region, providing suitable conditions for the maintenance of the potential vorticity ring and generating a feedback process. Meanwhile, the contribution of diabatic heating is largely offset by both the horizontal and vertical PV advections.

To gain more physical insights, we use the Sawyer–Eliassen model to investigate the effect of diabatic

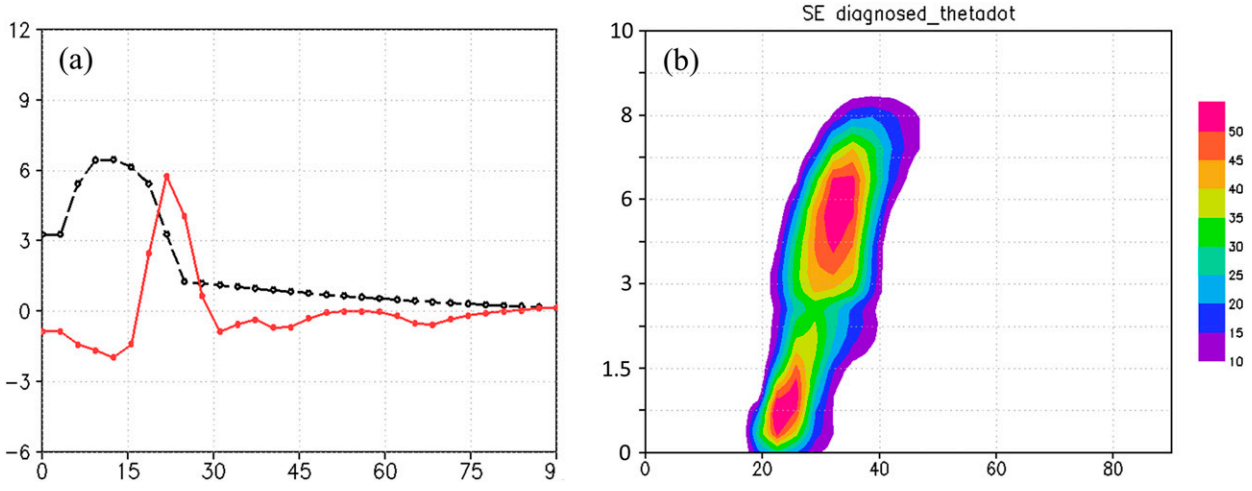

FIG. 8. (a) The initial iCTL vorticity profile ($s^{-1} \times 10^{-3}$; black line) and the initial diagnosed vorticity tendency ($s^{-1}\,h^{-1} \times 10^{-3}$; red line) in iCTL at $z = 3$ km. (b) The diabatic heating profile at 3 h and azimuthal-mean WRF output ($K\,h^{-1}$) provided for SE model diagnoses.

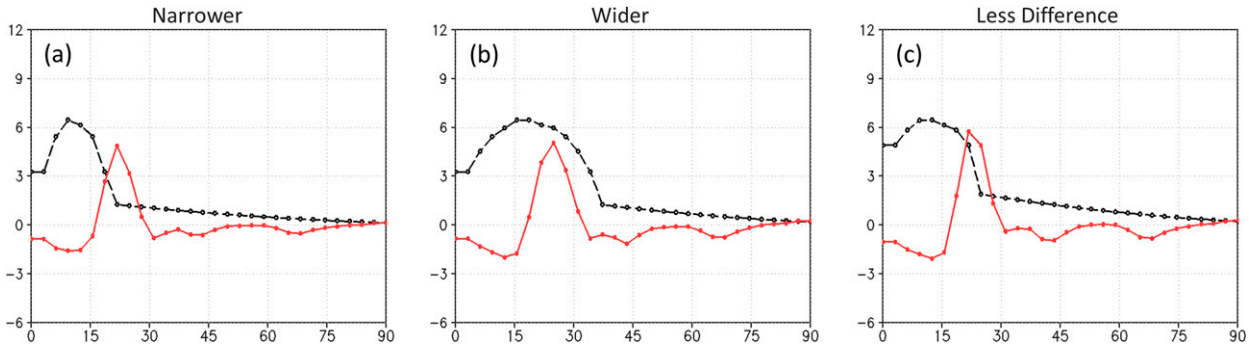

FIG. 9. The initial vorticity ($s^{-1} \times 10^{-3}$; black line) ring structures and the diagnosed vorticity tendency ($s^{-1}\,h^{-1} \times 10^{-3}$; red line) in sensitivity experiments of (a) NR, (b) WD, and (c) LD.

heating on the ring structure evolution. The results show that a ringlike vorticity tendency exists when diabatic heating is present. The initial ring structure, with either a narrower ring or with more vorticity difference between the ring and its center, has smaller positive vorticity tendencies in the ring area. Meanwhile, larger diabatic heating results in higher positive values of vorticity tendency in the ring region. Results from the sensitivity experiments suggest that, as long as sufficient diabatic heating is provided, eyewall ring structures should be sustained. This analysis points out that the presence of diabatic heating in the eyewall ring structure evolution, which is neglected by those 2D unforced-barotropic models, is pivotal to the eyewall evolutions.

In all, the two major findings in this study are as follows: 1) in numerical simulations where the intensity of the storms has reached the mature stage, and with enough convective heating, the eyewall ring is capable of maintaining its ringlike structure; and 2) the secondary circulation, induced by diabatic heating, is important to the maintenance of the annular structure. Although the high-resolution full-physics model can reasonably simulate the storm eyewall evolution, several unsolved problems related to eyewall structure evolution remain, such as how different initial ring structures affect the structure evolution in the 3D full-physics model, what role the friction and boundary layer play in affecting the ring structure evolution, and what parameters decide the ring structure evolution in a 3D full-physics simulation (i.e., the shape and the location of vorticity generation). Further investigations are needed to provide further insights to the above issues.

Acknowledgments. This work is supported by the Ministry of Science and Technology of Taiwan under Grants MOST 103-2628-M-002-004. Valuable comments from three anonymous reviewers that helped improve the quality of the manuscript are highly appreciated.

REFERENCES

Abarca, S. F., and M. T. Montgomery, 2014: Departures from axisymmetric balance dynamics during secondary eyewall formation. *J. Atmos. Sci.*, **71**, 3723–3738, doi:10.1175/JAS-D-14-0018.1.

——, and ——, 2015: Are eyewall replacement cycles governed largely by axisymmetric balance dynamics? *J. Atmos. Sci.*, **72**, 82–87, doi:10.1175/JAS-D-14-0151.1.

Bui, H. H., R. K. Smith, M. T. Montgomery, and J. Peng, 2009: Balanced and unbalanced aspects of tropical cyclone intensification. *Quart. J. Roy. Meteor. Soc.*, **135**, 1715–1731, doi:10.1002/qj.502.

Eliassen, A., 1951: Slow thermally or frictionally controlled meridional circulation in a circular vortex. *Astrophys. Norv.*, **5**, 19–60.

Guinn, T. A., and W. H. Schubert, 1993: Hurricane spiral bands. *J. Atmos. Sci.*, **50**, 3380–3403, doi:10.1175/1520-0469(1993)050<3380:HSB>2.0.CO;2.

Hack, J. J., and W. H. Schubert, 1986: Nonlinear response of atmospheric vortices to heating by organized cumulus convection. *J. Atmos. Sci.*, **43**, 1559–1573, doi:10.1175/1520-0469(1986)043<1559:NROAVT>2.0.CO;2.

Hendricks, E. A., and W. H. Schubert, 2010: Adiabatic rearrangement of hollow PV towers. *J. Adv. Model. Earth Syst.*, **2** (8), doi:10.3894/JAMES.2010.2.8.

——, M. T. Montgomery, and C. A. Davis, 2004: The role of "vortical" hot towers in the formation of Tropical Cyclone Diana (1984). *J. Atmos. Sci.*, **61**, 1209–1232, doi:10.1175/1520-0469(2004)061<1209:TROVHT>2.0.CO;2.

——, W. H. Schubert, R. K. Taft, H. Wang, and J. P. Kossin, 2009: Life cycles of hurricane-like vorticity rings. *J. Atmos. Sci.*, **66**, 705–722, doi:10.1175/2008JAS2820.1.

——, ——, Y.-H. Chen, H.-C. Kuo, and M. S. Peng, 2014: Hurricane eyewall evolution in a forced shallow-water model. *J. Atmos. Sci.*, **71**, 1623–1643, doi:10.1175/JAS-D-13-0303.1.

Hong, S.-Y., J. Dudhia, and S.-H. Chen, 2004: A revised approach to ice microphysical processes for the bulk parameterization of clouds and precipitation. *Mon. Wea. Rev.*, **132**, 103–120, doi:10.1175/1520-0493(2004)132<0103:ARATIM>2.0.CO;2.

Huang, Y.-H., M. T. Montgomery, and C.-C. Wu, 2012: Concentric eyewall formation in Typhoon Sinlaku (2008). Part II: Axisymmetric dynamical processes. *J. Atmos. Sci.*, **69**, 662–674, doi:10.1175/JAS-D-11-0114.1.

Janjić, Z., 2001: Nonsingular implementation of the Mellor–Yamada level 2.5 scheme in the NCEP MESO model. NOAA/NWS/NCEP Office Note 437, 61 pp. [Available

online at http://www.emc.ncep.noaa.gov/officenotes/newernotes/on437.pdf.]

Jordan, C. L., 1958: Mean soundings for the West Indies area. *J. Atmos. Sci.*, **15**, 91–97, doi:10.1175/1520-0469(1958)015<0091:MSFTWI>2.0.CO;2.

Kossin, J. P., and M. D. Eastin, 2001: Two distinct regimes in the kinematic and thermodynamic structure of the hurricane eye and eyewall. *J. Atmos. Sci.*, **58**, 1079–1090, doi:10.1175/1520-0469(2001)058<1079:TDRITK>2.0.CO;2.

——, and W. H. Schubert, 2001: Mesovortices, polygonal flow patterns, and rapid pressure falls in hurricane-like vortices. *J. Atmos. Sci.*, **58**, 2196–2209, doi:10.1175/1520-0469(2001)058<2196:MPFPAR>2.0.CO;2.

Möller, J. D., and M. T. Montgomery, 1999: Vortex Rossby waves and hurricane intensification in a barotropic model. *J. Atmos. Sci.*, **56**, 1674–1687, doi:10.1175/1520-0469(1999)056<1674:VRWAHI>2.0.CO;2.

Montgomery, M. T., and R. J. Kallenbach, 1997: A theory for vortex Rossby-waves and its application to spiral bands and intensity changes in hurricanes. *Quart. J. Roy. Meteor. Soc.*, **123**, 435–465, doi:10.1002/qj.49712353810.

——, M. E. Nicholls, T. A. Cram, and A. B. Saunders, 2006: A vortical hot tower route to tropical cyclogenesis. *J. Atmos. Sci.*, **63**, 355–386, doi:10.1175/JAS3604.1.

Naylor, J., and D. A. Schecter, 2014: Evaluation of the impact of moist convection on the development of asymmetric inner core instabilities in simulated tropical cyclones. *J. Adv. Model. Earth Syst.*, **6**, 1027–1048, doi:10.1002/2014MS000366.

Nguyen, M. C., M. J. Reeder, N. E. Davidson, R. K. Smith, and M. T. Montgomery, 2011: Inner-core vacillation cycles during the intensification of Hurricane Katrina. *Quart. J. Roy. Meteor. Soc.*, **137**, 829–844, doi:10.1002/qj.823.

Rotunno, R., and K. A. Emanuel, 1987: An air–sea interaction theory for tropical cyclones. Part II: Evolutionary study using a nonhydrostatic axisymmetric numerical model. *J. Atmos. Sci.*, **44**, 542–561, doi:10.1175/1520-0469(1987)044<0542:AAITFT>2.0.CO;2.

Rozoff, C. M., J. P. Kossin, W. H. Schubert, and P. J. Mulero, 2009: Internal control of hurricane intensity variability: The dual nature of potential vorticity mixing. *J. Atmos. Sci.*, **66**, 133–147, doi:10.1175/2008JAS2717.1.

——, D. S. Nolan, J. P. Kossin, F. Zhang, and J. Fang, 2012: The roles of an expanding wind field and inertial stability in tropical cyclone secondary eyewall formation. *J. Atmos. Sci.*, **69**, 2621–2643, doi:10.1175/JAS-D-11-0326.1.

Schubert, W. H., and J. J. Hack, 1983: Transformed Eliassen balanced vortex model. *J. Atmos. Sci.*, **40**, 1571–1583, doi:10.1175/1520-0469(1983)040<1571:TEBVM>2.0.CO;2.

——, M. T. Montgomery, R. K. Taft, T. A. Guinn, S. R. Fulton, J. P. Kossin, and J. P. Edwards, 1999: Polygonal eyewalls, asymmetric eye contraction, and potential vorticity mixing in hurricanes. *J. Atmos. Sci.*, **56**, 1197–1223, doi:10.1175/1520-0469(1999)056<1197:PEAECA>2.0.CO;2.

Shapiro, L. J., and H. E. Willoughby, 1982: The response of balanced hurricanes to local sources of heat and momentum. *J. Atmos. Sci.*, **39**, 378–394, doi:10.1175/1520-0469(1982)039<0378:TROBHT>2.0.CO;2.

Skamarock, W. C., and Coauthors, 2008: A description of the Advanced Research WRF version 3. NCAR Tech. Note NCAR/TN-475+STR, 113 pp. [Available online at http://www2.mmm.ucar.edu/wrf/users/docs/arw_v3.pdf.]

Van Sang, N., R. K. Smith, and M. T. Montgomery, 2008: Tropical-cyclone intensification and predictability in three dimensions. *Quart. J. Roy. Meteor. Soc.*, **134**, 563–582, doi:10.1002/qj.235.

Wang, Y., 2009: How do outer spiral rainbands affect tropical cyclone structure and intensity? *J. Atmos. Sci.*, **66**, 1250–1273, doi:10.1175/2008JAS2737.1.

——, and C. C. Wu, 2004: Current understanding of tropical cyclone structure and intensity changes—A review. *Meteor. Atmos. Phys.*, **87**, 257–278, doi:10.1007/s00703-003-0055-6.

Willoughby, H. E., J. A. Clos, and M. G. Shoreibah, 1982: Concentric eye walls, secondary wind maxima, and the evolution of the hurricane vortex. *J. Atmos. Sci.*, **39**, 395–411, doi:10.1175/1520-0469(1982)039<0395:CEWSWM>2.0.CO;2.

Wu, C.-C., H.-J. Cheng, Y. Wang, and K.-H. Chou, 2009: A numerical investigation of the eyewall evolution in a landfalling typhoon. *Mon. Wea. Rev.*, **137**, 21–40, doi:10.1175/2008MWR2516.1.

Yau, M. K., Y. Liu, D.-L. Zhang, and Y. Chen, 2004: A multiscale numerical study of Hurricane Andrew (1992). Part VI: Small-scale inner-core structures and wind streaks. *Mon. Wea. Rev.*, **132**, 1410–1433, doi:10.1175/1520-0493(2004)132<1410:AMNSOH>2.0.CO;2.